CITATION

Warner, S.J., J. Becherer, K. Pujiana, E.L. Shroyer, M. Ravichandran, V.P. Thangaprakash, and J.N. Moum. 2016. Monsoon mixing cycles in the Bay of Bengal: A year-long subsurface mixing record. *Oceanography* 29(2):158–169, http://dx.doi.org/10.5670/oceanog.2016.48.

DOI

http://dx.doi.org/10.5670/oceanog.2016.48

Monsoon Mixing Cycles in the Bay of Bengal

A Year-Long Subsurface Mixing Record

By Sally J. Warner,
Johannes Becherer,
Kandaga Pujiana,
Emily L. Shroyer,
M. Ravichandran,
V.P. Thangaprakash,
and James N. Moum

Photo credit: James N. Moum

ABSTRACT. Based on the first year-long record of mixing collected in the eastern central Bay of Bengal, we quantify the role that subsurface turbulent heat fluxes play in upper-ocean cooling brought on by southwest (SW) and northeast (NE) monsoons. During the NE (dry, or winter) monsoon, atmospheric and subsurface turbulent heat fluxes each contribute about 50% of the net sea surface cooling. During the SW (wet, or summer) monsoon, the atmospheric heat flux varied widely due to "active" and "break" cycles of the monsoon intraseasonal oscillations, but had a net positive seasonal average. The subsurface turbulent heat flux during the SW monsoon led to surface cooling at rates more than three times greater than those measured during the NE monsoon. Since the seasonally averaged atmospheric heat flux was positive, subsurface mixing accounted for nearly all of the cooling during the SW monsoon. During the transition between the NE and SW monsoons, subsurface heat flux was near zero, and atmospheric heating rapidly warmed the sea surface. Following the SW monsoon, passage of Tropical Storm Hudhud led to $O(1)$ m^2 s^{-1} rates of turbulence diffusivity and strong subsurface heat flux, accounting for roughly half of the 1.4°C surface cooling that occurred over a 60-hour period.

INTRODUCTION

The South Asian monsoon is a system of periodically reversing winds and precipitation that is regulated by seasonal migration of the intertropical convergence zone (ITCZ; Gadgil, 2003). The ITCZ is located in the Northern Hemisphere over the South Asian subcontinent in boreal summer, and the lower limb of the Hadley circulation drives energetic southwesterly winds across the Bay of Bengal (BoB). Moisture accumulates as the southwesterly winds pass over warm surface waters of the BoB, bringing heavy rainfall to northern India (Bhat et al., 2001). During the southwest (SW) monsoon, rainfall is not continuous but is characterized by variability at 10–20 day and 30–60 day (intraseasonal) time scales that govern the "active" (wet) and "break" (dry) cycles of the monsoon (Sengupta and Ravichandran, 2001; Sengupta et al., 2001; Goswami, 2011). In boreal winter, the ITCZ retreats to the Southern Hemisphere and the dry, northeasterly winds of the northeast (NE) monsoon transit over the BoB, accumulating moisture and bringing rain to regions of southern India and northeastern Sri Lanka (Gadgil, 2003). During the monsoon transition period between the NE and SW monsoons, calm winds set up over the region.

In the BoB, barrier layers with strong salinity stratification and negative temperature gradients between the base of the mixed layer and the thermocline form periodically on both short and long time scales and large and small spatial scales (Thadathil et al., 2002, 2007; Girishkumar et al., 2011; Agarwal et al., 2012). Precipitation and riverine input are the main sources of freshwater in barrier layers, and processes such as wind, local currents (Thadathil et al., 2007), and westward-propagating Rossby waves (Girishkumar et al., 2011) can modify and dissipate barrier layers. Consequent reversing temperature gradients result in mixing upward of water that can both warm and cool the sea surface (de Boyer Montégut et al., 2007). The alternating sign of the turbulent heat flux in part distinguishes the role of subsurface fluxes to sea surface modification between alternating monsoon seasons.

Because of the influence of the monsoons on local weather, particularly precipitation, accurate prediction of the monsoon is a priority for BoB rim countries. However, the South Asian monsoon is a particularly difficult phenomenon for climate models to predict accurately (Syed et al., 2014). Good estimates of surface fluxes are considered a necessity in predicting large-scale air-sea interactions that contribute to coupled systems such as the South Asian monsoons,

but these values can be difficult to constrain (Schott et al., 2009). It is even more challenging to estimate subsurface fluxes and their contributions to surface properties using observations. BoB heat budgets have been computed in the past. For example, Loschnigg and Webster (2000) used a model that parameterized vertical mixing, showing that lateral transport and storage balance surface heat fluxes. Shenoi et al. (2002) used climatological temperatures and surface heat fluxes and assumed a constant diffusivity at the base of a 50 m deep mixed layer, and found diffusive fluxes ranging between –35 W m^{-2} and –60 W m^{-2}. Sengupta et al. (2002) used data collected from a mooring in the central BoB to estimate a springtime heat budget of the mixed layer. They estimated residual cooling due to vertical mixing and advection to be about –25 W m^{-2}. de Boyer Montégut et al. (2007) use a global ocean general circulation model to highlight the importance of barrier layers in the BoB that allow negative temperature gradients in regions of strong salinity stratification. Girishkumar et al. (2013) also highlight the importance of barrier layers in their calculation of a wintertime heat budget using mooring data. They found subsurface heat fluxes using a constant diffusivity between November and February of –23 ± 15 and –10 ± 4 W m^{-2} in two subsequent years. Most recently, as part of the Air-Sea Interactions Regional Initiative (ASIRI; Goswami et al., 2016, in this issue), investigations of air-sea interactions (Weller et al., 2016, in this issue) and mixed layer heat budgets (Thangaprakash et al., 2016, in this issue) were carried out. In all of these studies, subsurface fluxes were either estimated using mixing parameterizations or calculated as a residual. Here, the first sustained measurements of subsurface mixing in the BoB were made from a number of moorings as part of ASIRI. Analysis of records from the first of these moorings to be recovered hints at the role subsurface turbulence plays in modifying surface properties.

MIXING DEPLOYMENTS IN THE BAY OF BENGAL 2013–2016

A number of oceanographic moorings in the BoB were outfitted with χpods as part of ASIRI (Figure 1). χpods are instruments developed to measure turbulence using fast thermistors (Moum and Nash, 2009; Perlin and Moum, 2012). They have provided insight into long-term variations in mixing from a range of locations in the Pacific (e.g., Moum et al., 2013), and numerous moorings in the BoB have been equipped with χpods since 2013. Five moorings deployed by the US Naval Research Laboratory in the southern BoB were outfitted with χpods for a one-year duration in 2013.

The Research Moored Array for African-Asian-Australian Monsoon Analysis and Prediction (RAMA) mooring at 12°N, 90°E (McPhaden et al., 2009b) included two χpods at 15 m and 30 m depths from late 2013 through late 2014. The χpod presence on the RAMA moorings was expanded in late 2014 to include three χpods in the upper 45 m at 8°N, 90°E[1]; 12°N, 90°E; and 15°N, 90°E. Additionally, the Woods Hole Oceanographic Institution (WHOI) monsoon buoy at 18°N, 90°E was equipped with χpods from November 2015 to January 2016.

The first records to be returned, and with a nearly complete set of complementary data, comes from the RAMA mooring at 12°N, 90°E, deployed in late 2013. With a measure of mean flow speed, frequency (derived from χpod time series) is converted to wavenumber in order to compare measured temperature spectra to empirical turbulence forms, thus permitting estimation of turbulence quantities representing the diffusive dissipation of small-scale temperature gradients (χ_T) and the turbulence diffusivity (K_T) where $K_T = \chi_T / (2T_z^2)$. The diffusivity is then combined with the local vertical temperature gradient (T_z) to calculate the vertical heat flux due to turbulence using

$$J_q^t = -\rho\, c_p\, K_T\, T_z, \qquad (1)$$

where ρ is density, c_p is specific heat, and the negative sign indicates the direction of heat flux with respect to the temperature gradient.

The RAMA mooring at 12°N, 90°E had a single velocity record immediately above the upper χpod at 12 m depth (SonTek Argonaut Doppler current meter). Complementary data also included temperature and conductivity measurements at 1 m (temperature only), 10 m, 20 m, 40 m, and 60 m depths. Due to the often-dominating influence of salinity on BoB stratification, good conductivity measurements are critical to accurate calculation of the buoyancy frequency, N^2.

THE SOUTH ASIAN MONSOONS OF 2014

Figure 2a–d compares time series of daily averaged wind stress (τ), precipitation (P), atmospheric (net surface) heat flux (J_q^0), and sea surface temperature (SST) from the RAMA mooring at 12°N, 90°E over the period of χpod deployment from late 2013 through late 2014 to climatological averages at 12°N, 90°E of τ, J_q^0, SST calculated from TropFlux over 1979–2015 (Praveen Kumar et al., 2012), and P from the National Centers for Environmental
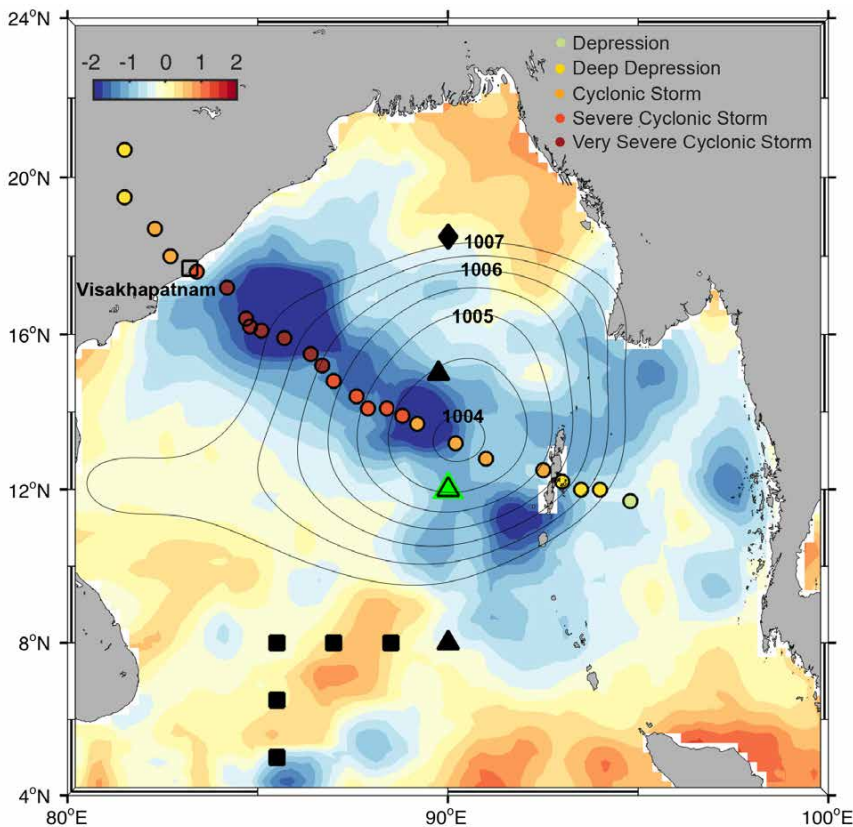

FIGURE 1. Locations of χpods in the Bay of Bengal: Research Moored Array for African-Asian-Australian Monsoon Analysis and Prediction (RAMA) mooring at 12°N, 90°E (green triangle), other RAMA moorings (black triangles), EBOB array from the US Naval Research Laboratory (black squares), and Ocean Mixing and Monsoon-Woods Hole Oceanographic Institution (OMM-WHOI) monsoon buoy (black diamond). The track of Tropical Storm Hudhud is shown with yellow, orange, and red dots corresponding to the Indian Meteorological Department Tropical Cyclone Intensity Scale (upper right). Also shown are contours of sea surface pressure (gray lines) on October 9, 2014, when the eye of Tropical Storm Hudhud was within 100 km of 12°N, 90°E. In the background is a composite image of the sea surface temperature (SST) anomaly (°C) from the Optimal Interpolation Sea Surface Temperature (OISST) analysis in the days following the passage of Hudhud across the BoB.

---

[1] Just prior to submission of the final revisions to this paper, we were informed that the 8°N, 90°E mooring was lost, together with all of our χpods.

Prediction reanalysis 1 (NCEP1) over 1948–2015 (Kalnay et al., 1996). No RAMA longwave radiation is available at this location, and the RAMA shortwave radiation ends on August 3, 2014. Daily averaged TropFlux values from 12°N, 90°E were used to replace the gaps in RAMA data (gray, Figure 2c). We do not anticipate this to incorporate significant errors because RAMA and TropFlux radiative fluxes have near-negligible mean biases (Praveen Kumar et al., 2012). Throughout our analysis, TropFlux climatology for net atmospheric heat flux (1979–2015) and the Objectively Analyzed air-sea Fluxes (OAFlux; 1985–2009; Yu and Weller, 2007) are used because they have the smallest systematic biases of all reanalysis products compared to RAMA measurements (Yu et al., 2007; McPhaden et al., 2009b; Praveen Kumar et al., 2012).

Figure 2 divides the deployment period into four significant regimes: NE monsoon (December 1, 2013–March 18, 2014, tan), transition (March 19–May 5, 2014, green), SW monsoon (May 6–September 24, 2014, blue), and Tropical Storm (TS) Hudhud (October 8–10, 2014, red). The beginning and end of each of these periods was determined by shifts in the amplitude of the wind stress and precipitation rate. In some studies, the NE and SW monsoons are defined temporally from November 1 through February 28 and June 1 through September 30, respectively. However, as Schott and McCreary (2001) point out, the onsets and terminations of the monsoons are variable, which is why we define starts and ends of the monsoons by physical phenomena here. The wind, precipitation, and water properties during each period have distinct characteristics and trajectories (Figures 2 and 3).

The NE monsoon was already established at the beginning of the χpod deployment on December 1, 2013, and continued until the wind stress systematically decreased on March 18, 2014. This period was dominated by northeasterly winds (Figure 4a), low precipitation (Figure 2b), and dry air.
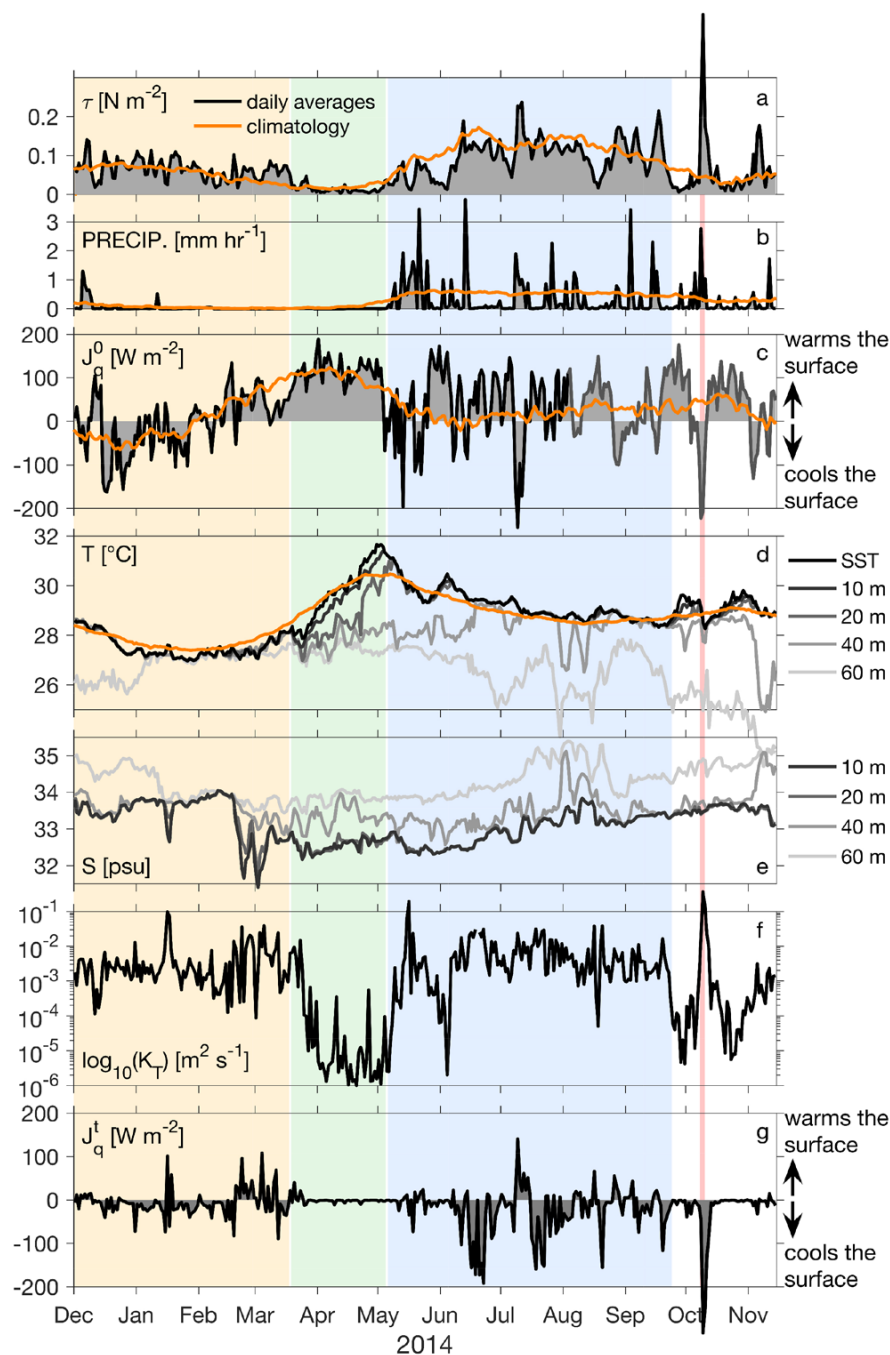

FIGURE 2. (a) Daily averaged surface wind stress (shaded in gray, outlined in black) from the RAMA mooring at 12°N, 90°E from December 1, 2013, through November 21, 2014. (b) Daily averaged precipitation rate. (c) Atmospheric (net surface) heat flux (J_q^0). TropFlux longwave radiation is used for the duration of the deployment and TropFlux shortwave radiation is used from August 3, 2014, onward after the RAMA shortwave radiation ends (gray outline). Negative (positive) values indicate heat flux out of (into) the ocean. (d) Sea surface (black) and subsurface temperatures at 10 m, 20 m, 40 m, and 60 m (grays). (e) Subsurface salinities at 10 m, 20 m, 40 m, and 60 m. (a–d) Climatological averages (orange) calculated from 1979–2015 TropFlux for wind stress, atmospheric heat flux, and temperature, and from 1948–2015 NCEP1 for precipitation. (f) Turbulence diffusivity (K_T) as measured by a χpod at 15 m depth. (g) Turbulent heat flux (J_q^t) at 15 m. Positive (negative) values indicate upward (downward) heat flux that warms (cools) the sea surface. Four time periods are highlighted with background shading: NE monsoon (December 1, 2013–March 18, 2014, tan), weak-wind and zero-precipitation transition between the NE and SW monsoons (March 19–May 5, 2014, green), SW monsoon (May 6–September 24, 2014, blue), and the passage of Tropical Storm Hudhud (October 8–10, 2014, red).

During December and January, negative daily averages of J_q^0 cooled the sea surface, and SST decreased from 28.5°C to 27°C. This cooling was not associated with a significant change in salinity (Figures 2e and 3). During February and the first half of March, northeasterly winds continued, although weaker in strength compared to the previous two months. Between February 17 and March 2, salinity at 10 m depth freshened from 33.9 psu to 31.4 psu (Figures 2e and 3), presumably due to advection of freshwater from the northeast (Figure 4c). Slight SST warming occurred in conjunction with combined atmospheric and subsurface heating (Figure 2c,g).

Following the NE monsoon, the transition period was characterized by low wind stress and zero precipitation from March 19 through May 5, 2014. Strong and steady atmospheric heating increased SST to almost 32°C (Figure 2a–d). The rapid rise in SST was associated with a very slight increase in salinity (Figures 2e and 3).

The ensuing SW monsoon (May 6 through September 24, 2014) provided significant contrasts to the NE monsoon. Wind stress was almost twice the magnitude as that during the NE monsoon, and precipitation was heavy but punctuated by dry spells associated with active and break cycles of the atmospheric monsoon intraseasonal oscillations (MISOs), which are evident in the variability of J_q^0 during this season (Figure 2a–c). Surface cooling proceeded quickly during May and then more slowly through the rest of the SW monsoon; SST reached a minimum value of a little less than 29°C in late September (Figures 2d and 3). Despite significant rainfall during the SW monsoon, the salinity at 10 m depth gradually and steadily increased from 32.3 psu in May to 33.5 psu in September (Figures 2e and 3). This suggests that mixing of saltier water from below may be a key process contributing to gradual increases in near-surface salinity.

The end of the deployment was dominated by TS Hudhud, which formed over the Andaman Sea and propagated WNW across the BoB, gaining energy from the upper ocean along its path—a typical growth pattern for tropical storms over a warm ocean (Emanuel, 2003). The eye of TS Hudhud passed within 100 km of our mooring site on October 9, 2014 (Figure 1). Hudhud was progressively upgraded (using the terminology of the Indian Meteorological Office) from Deep Depression as it passed our mooring site to Cyclonic Storm and Severe Cyclonic Storm, reaching Very Severe Cyclonic Storm (equivalent to a category 4 storm on the Saffir-Simpson Scale) as it approached Visakhapatnam, India. Tropical Cyclone (TC) Hudhud made landfall on October 12, 2014, at 10:25 am local time (Fritz, 2014), causing considerable loss of life and property damage. In all, over two million people were affected by the storm, with 46 deaths confirmed in the coastal state of Andhra Pradesh (*The Times of India*, 2014). Another 43 people were killed by an avalanche in Nepal on October 14, which was brought on by blizzard conditions associated with TC Hudhud as it moved northward over land (Wang et al., 2015). Maximum sustained wind speeds of 175 km h^{-1} (109 mph), gusts of 260 km h^{-1} (160 mph) (Fritz, 2014),
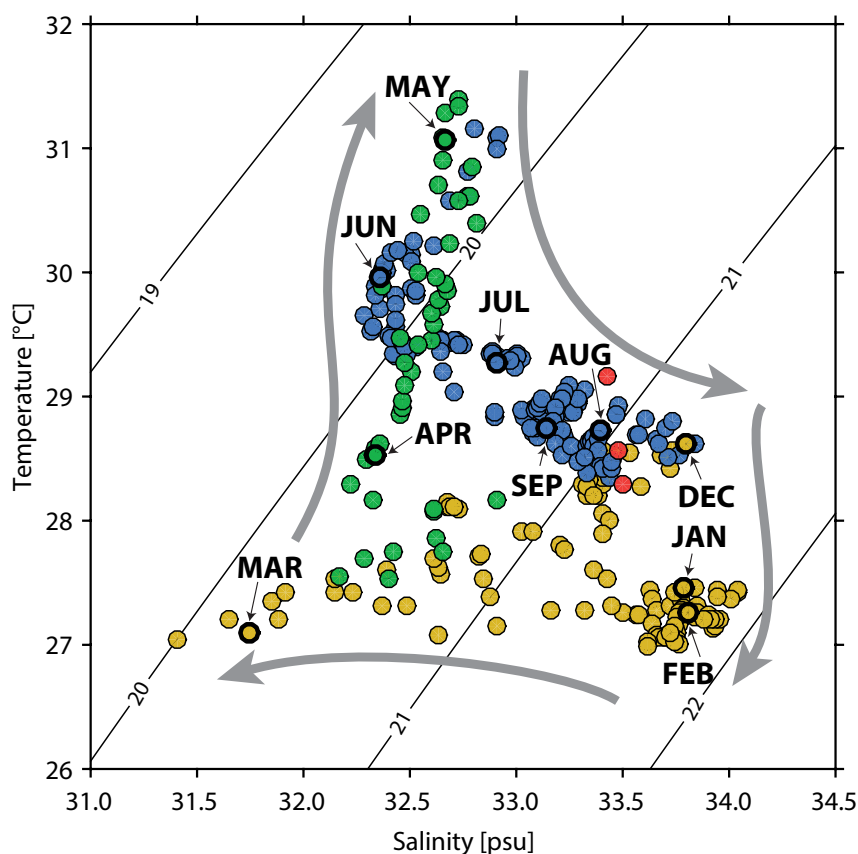

FIGURE 3. Daily averaged temperature and salinity at 10 m depth from December 1, 2013, through September 24, 2014, and October 8–10, 2014. The first days of each month are indicated with arrows and plotted with thicker outlines. The general progression in time is shown with the gray arrows. The water initially cools from December to January during the NE monsoon (tan), then saltier water is advected into the analysis region during February, leading to a much fresher March. During the March through May transition (green), the water warms and there is a slight increase in salinity. The SW monsoon (blue) initially cools rapidly and slightly freshens the water in May; then in June through September, the water continues to cool and there is a gradual but steady increase in salinity. Finally, during Tropical Storm Hudhud in early October (red), the water at 10 m depth cooled significantly over the three-day period of the storm's passage. The salinity also increased slightly, indicative of mixing of saline waters from below.

and a storm surge of 3.5 m (11.5 feet) were recorded in Visakhapatnam (Gaulter, 2014). The United Nations estimates damages due to TC Hudhud to be $11 billion USD and credits the Indian government with saving many lives by timely evacuating nearly 500,000 people from the state of Andhra Pradesh (*The Economic Times*, 2015).

UPPER-OCEAN CURRENTS AT 12°N, 90°E

Variations in magnitude and direction of monsoonal winds drive variations in near-surface currents and distinctly different velocity regimes at 12 m depth (Figure 4). The NE monsoon was characterized by strong and constant mean flow to the northwest, consistent with Ekman transport forced by steady northeasterly monsoon winds. Conversely, during the SW monsoon, the mean current pattern was generally weaker and more variable, and cannot be simply linked to Ekman transport alone.

A spectrogram of velocity shows most of the kinetic energy to be distributed in three distinct bands: near inertial (near-f), diurnal, and semidiurnal (M_2; Figure 4d). Presumably associated with internal tides, the energy in the semidiurnal band occurs throughout the entire record, independent of wind forcing. Near-f energy is mainly driven by atmospheric forcing. Strong southwesterly wind bursts during the SW monsoon (Figure 4a) appear in the wind stress spectrogram (Figure 4b) as broadband excitations. These wind bursts occur approximately every 25 to 30 days and are linked to the MISOs. Coincident with the wind bursts are near-f peaks in the current spectrogram (Figure 4d), indicating that each atmospheric broadband excitation deposits a substantial amount of energy in the near-f band of the surface currents (Figure 4d).

The most energetic event in the record is TS Hudhud, with peak wind stress of 1 N m^{-2} and current velocities almost 1 m s^{-1}. Most of the energy in the storm is at relatively low frequencies (Figure 4b). The initial ocean current response is subinertial, but quickly shifts toward the inertial band.

When looking at the spectrogram of the wind stress (Figure 4b), it is interesting to note that the tropical cyclone appears
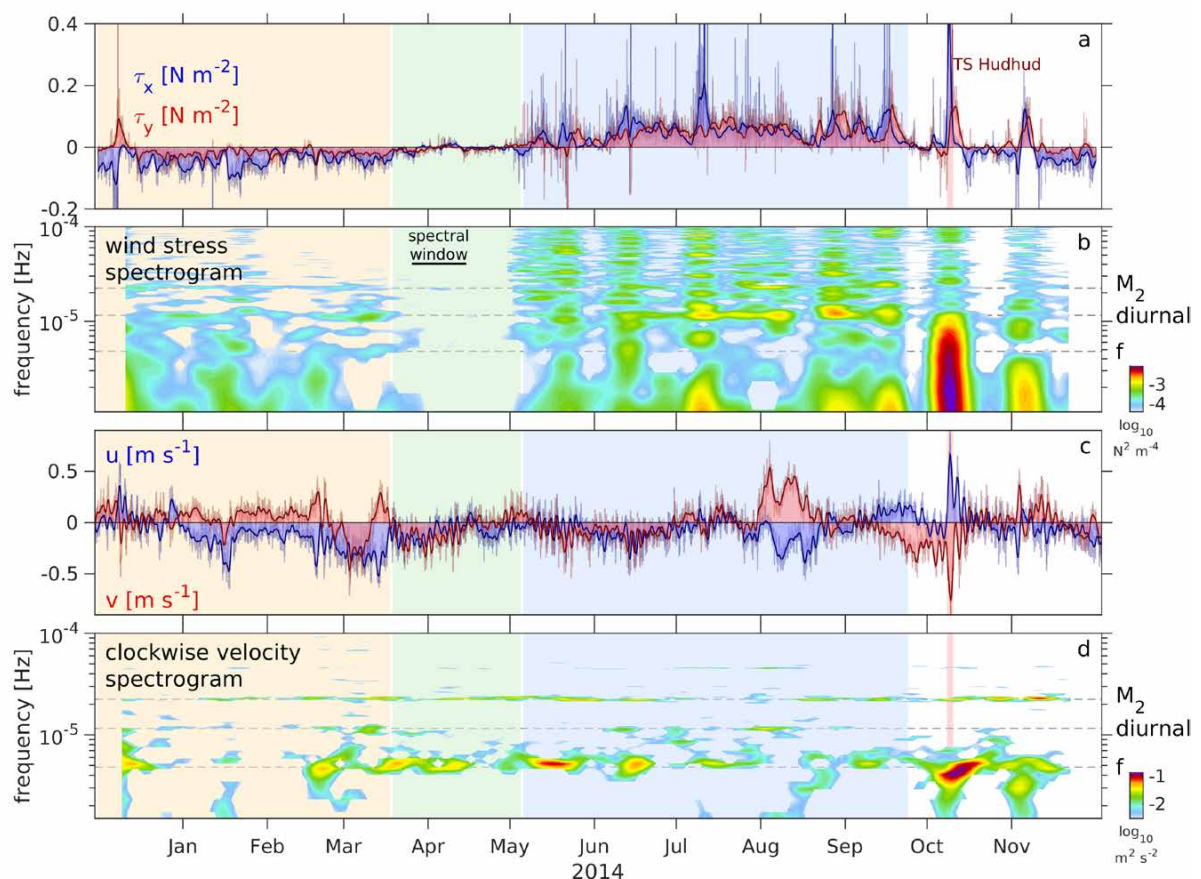

FIGURE 4. (a) Eastward (blue) and northward (red) components of wind stress from RAMA, corresponding to westerly and southerly winds, respectively. (c) Eastward (blue) and northward (red) components of current velocity at 12 m depth from RAMA. For both velocity and wind stress, the thick dark lines correspond to a one-day low-pass filtered signal and the thin light lines to the high-frequency sample (currents 30 min and wind 10 min). (b, d) Spectrograms of wind stress (b) and velocity (d), calculated with a 20-day spectral window that is consecutively shifted by two days. Note that (d) only shows the clockwise part of the spectrum, whereas (b) displays the sum of both components. The shaded background indicates the different periods: NE monsoon (tan), SW monsoon (blue), transition (green), and TS Hudhud (red).

as a final disturbance in a sequence of southwesterly wind bursts related to the MISOs. While this is possibly random coincidence, the timing may also hint at a connection between cyclones and MISOs, where the two may at times interact with one another. (However, many cyclones develop within the NE monsoon outside of the boreal summer MISO period.) We note the occurrence of a second weaker cyclone not quite 30 days after Hudhud at the beginning of November, which also fits the sequence of southwesterly wind bursts.

MONSOON MIXING CYCLES

The unique part of this moored record is the long time series of mixing at 15 m depth (Figure 2f,g). Variations in K_T (Figure 5) and J_q^t (Figure 6) are significant and systematic.

The early part of the NE monsoon is characterized by K_T values of $O(10^{-3})$ m^2 s^{-1} (Figure 2f). These diffusivity values are two orders of magnitude greater than deep-ocean diffusivity estimates (Toole et al., 1994), but typical of upper-ocean magnitudes. The sign of T_z defines the sign of J_q^t. With T_z generally increasing toward the surface, the mixing of cooler waters upward from below cools the sea surface ($T_z > 0$ and $J_q^t < 0$). J_q^t cools the surface during the first three-quarters of the NE monsoon (Figure 2g). Toward late February, surface currents changed speed and direction. Weaker currents from the south were replaced by stronger currents from the north (Figure 4c). Water advected

by these currents was associated with fresher surface waters (Figure 2e), the development of a barrier layer (Thadathil et al., 2007), and a change in sign of T_z. In response, J_q^t changed from cooling to heating of the sea surface from below. There was also a week in mid-January where an intrusion of low-saline waters correlated with spikes in K_T and positive J_q^t. Similar dynamics for subsurface vertical heat flux with and without temperature inversions have previously been observed in the BoB (Girishkumar et al., 2013). The larger values of K_T were presumably due to greater current shear and enhanced shear instability, although we do not have sufficient information to test this hypothesis. Toward the end of the NE monsoon, both J_q^0 and J_q^t contributed to heating the sea surface; SST increased by about 1°C.

Despite the late season change in sign, when averaged over the NE monsoon, J_q^0 weakly cooled the sea surface, and the mean of J_q^0 (–7 W m^{-2}) showed slightly more surface cooling than the seasonally averaged climatological surface heat flux from TropFlux (+1 W m^{-2}) and OAFlux (–1 W m^{-2}) (Figure 6). Averaged J_q^t (–7 W m^{-2}) during the NE monsoon was weakly negative, contributing nearly the same amount of cooling of surface waters as J_q^0. The late season change in sign in late February and early March countered the predominantly negative heat flux in December, January, and early February. As a comparison, a mixed layer heat budget, using RAMA mooring data from 8°N, 90°E and a constant

K_T to estimate turbulent heat fluxes, found November–February averages of –23 ± 15 W m^{-2} and –10 ± 4 W m^{-2} during 2006–2007 and 2007–2008, respectively (Girishkumar et al., 2013).

Strong atmospheric heating during the transition (Figure 2c) was the principal reason for greatly increased near-surface stratification and the nearly complete isolation of the ocean at 15 m depth from weak surface forcing. Vertical salinity gradients at 15 m depth during this period were near zero (Figure 2d). Daily averaged values of K_T decreased to near-noise levels for almost two months (Figure 2f). The increase in SST can be fully attributed to J_q^0 during this period. This result contrasts that of Sengupta et al. (2002) who calculate a March to May heat budget of the northern BoB using buoy data. Despite similar measurements of J_q^0, their estimate of residuals (combination of advection and vertical mixing) required to maintain mixed layer temperatures is –25 W m^{-2}, much greater in magnitude than our observations.

During the SW monsoon, K_T was larger by a factor of two to five than during the NE monsoon and included a spike in mid-May of $>10^{-1}$ m^2 s^{-1} at the onset of the first strong wind following the spring warming (Figures 2f and 5). J_q^t was primarily negative (Figure 2g). A week-long period of positive J_q^t occurred in early July at the same time as a burst of strong westerly winds (Figure 4a) and a drop in near-surface salinity (Figure 2e)—similar to the sequence of events that resulted in a change in sign of J_q^t during
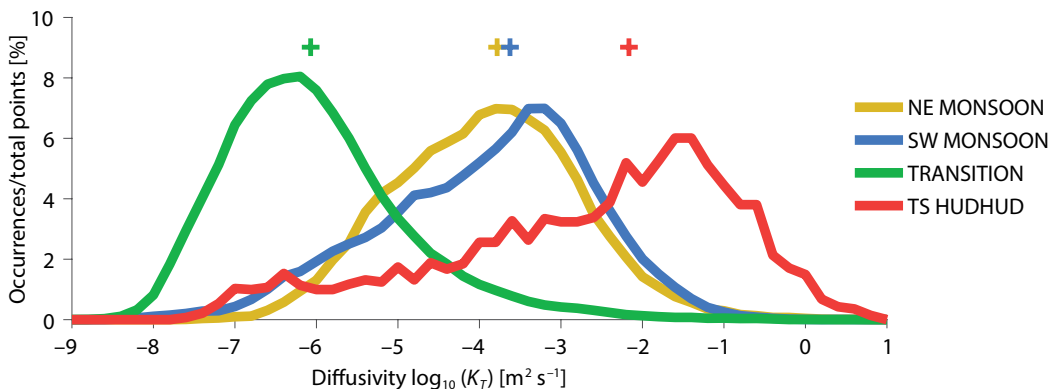
the NE monsoon.

The distribution of daily averaged values of J_q^0 fluctuated widely between –250 to +200 W m^{-2} during the SW monsoon, covering a much larger magnitude range and having a higher percentage of positive values compared to the NE monsoon (Figure 6a). The seasonally averaged value of J_q^0 during the SW monsoon was +30 W m^{-2}, which was within the range of climatological averages of J_q^0 over the same period (TropFlux = +21 W m^{-2}, OAFlux = +34 W m^{-2}; Figure 6b). Turbulent heat flux during the SW monsoon was predominately negative, with a seasonal average of J_q^t = –22 W m^{-2}. This means that during the SW monsoon, despite the occurrence of occasional break cycles, the net value of J_q^0 was positive, and therefore J_q^t was the key one-dimensional process controlling cooling of surface waters.

From a heat budget analysis of the upper 50 m in the BoB using various climatological data and a constant K_T to estimate vertical diffusive fluxes, Shenoi et al. (2002) found J_q^t to be roughly –50 W m^{-2} during the SW monsoon. While this is larger than our measured average, Shenoi et al. (2002) showed a similar annual trend with twice as much diffusive flux during the SW monsoon than during the NE monsoon.

Differences in K_T during the four time periods are represented by histograms in Figure 5. The transition period and TS Hudhud represent extrema; differences in distribution modes are >5 orders of magnitude. These extrema clearly differentiate the monsoons. However, significant differences in distributions of K_T also exist between the SW and NE monsoons, with a higher predominance of $K_T > 10^{-3}$ m^2 s^{-1} and $K_T < 10^{-6}$ m^2 s^{-1} occurring during the SW monsoon. Taken together with the differing signs of T_z between the two monsoons, these differences demonstrate the varying role that subsurface mixing plays in sea surface modification during the SW and NE monsoons (Figure 6).

The critical distinction between the NE and SW monsoons is that turbulent mixing augments weak surface cooling during the NE monsoon (apart from cyclone activity—see below), and during the SW monsoon, turbulent mixing counteracts strong atmospheric warming and is therefore the dominant one-dimensional process working to cool the surface.

TROPICAL STORM HUDHUD

Heat transferred from the ocean drives tropical cyclones; therefore, vertical mixing in the upper ocean provides an essential negative feedback to these storms (Emanuel, 2003; Yu and McPhaden, 2011). TS Hudhud passed less than 100 km to the north of 12°N, 90°E on October 8–10, 2014, while still classified as a tropical storm (Figure 1). A composite image of the Optimal Interpolation Sea Surface Temperature (OISST) anomaly from the Advanced Very High Resolution Radiometer satellite (AVHRR; Reynolds et al., 2007) shows a distinct drop in SST of ~2°C–3°C to the right of the eye of Hudhud over the five days it took Hudhud to cross the BoB preceding landfall on October 12, 2014, near Visakhapatnam, India (Figure 1). Large sea surface impacts to the right of the eye of the storm in the Northern Hemisphere are typical (D'Asaro et al., 2007), and decreases in SST of this
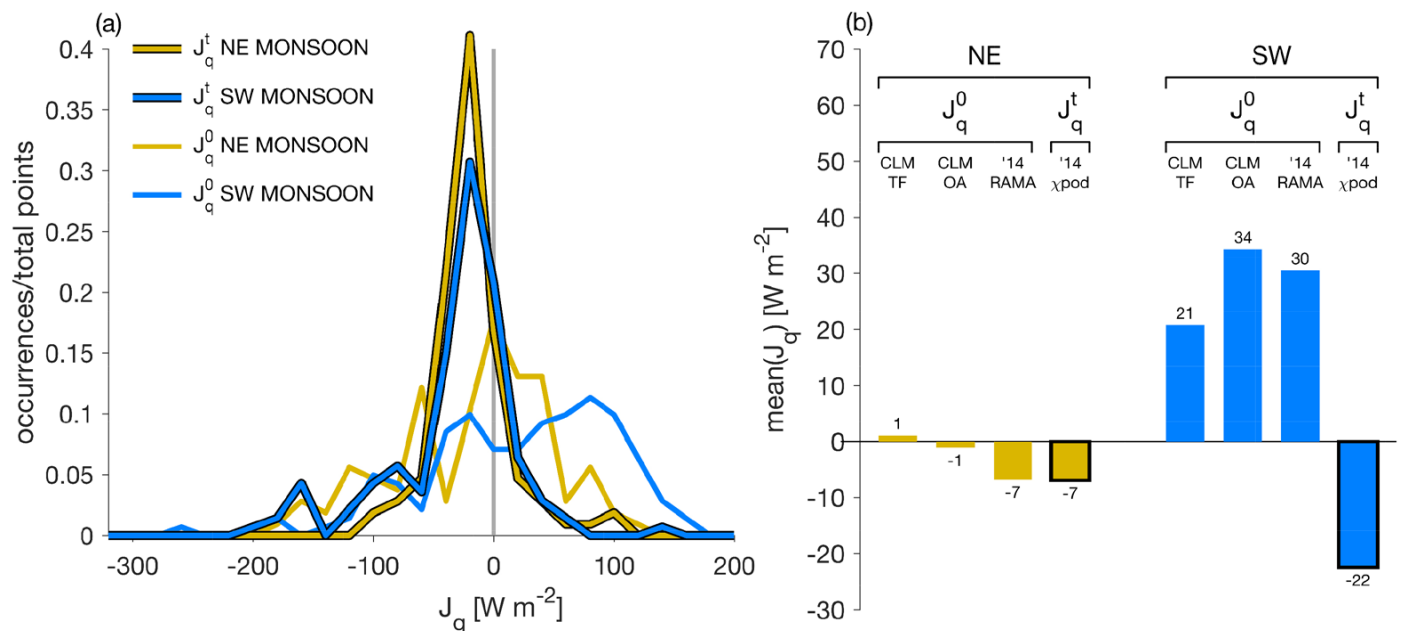

FIGURE 6. (a) Histograms of daily averaged atmospheric heat flux from RAMA (J_q^0, thin lines) and subsurface turbulent heat flux from χpods (J_q^t, thick lines with black edges) during the NE (107 days, tan) and SW (141 days, blue) monsoons. Positive values indicate heat flux into surface waters. (b) Seasonally averaged heat fluxes during the NE (tan) and SW monsoons (blue): climatology of atmospheric heat fluxes from TropFlux (J_q^0 CLM TF) and OAFlux (J_q^0 CLM OA), observed atmospheric heat fluxes from RAMA (J_q^0 '14 RAMA), and observed turbulent heat fluxes (J_q^t '14 χpod, black outline).

Science Box: How Do You Find a χpod?

Sometimes a picture really is worth a thousand words.

After being deployed from November 2013 through December 2014 on the RAMA mooring at 12°N, 90°E, two χpods—along with lots of other scientific instrumentation—were placed in a large sea container belonging to the US National Oceanic and Atmospheric Administration Pacific Marine Environmental Laboratory (PMEL) on the campus of the National Institute of Ocean Technology (NIOT) in Chennai, India. Eventually this container will be shipped back to the United States, but because of Indian regulations regarding the shipping of hazardous materials and a large flood that hit Chennai in November 2015 that left the NIOT campus severely flooded, the container was still in India a year after recovery. This meant that data recorded by the χpods had yet to be analyzed and viewed by curious scientists at home in Oregon.

In late December 2015, Pavan Vutukur, an electronics engineer who works in our group at Oregon State University and who grew up in Hyderabad, India, visited Chennai with a laptop and an SD card reader to retrieve the data. This is how he tells the story of the day:

"Things started out well. I reached NIOT and met up with Suresh Kumar who is a scientist and engineer at the Indian National Centre for Ocean Information Services at NIOT. He introduced me to his team of workers that would remove the χpod boxes from the PMEL container. However, I got nervous when the workers opened the container. It was packed to the brim with various boxes and oceanographic instrumentation and the χpod boxes were buried deep inside!

"The NIOT folks started asking me what type of instruments I was looking for and what boxes they would be in. This was not as easy to explain as one would think! I grew up in Hyderabad where the local language is Telugu, but the local language in Chennai is Tamil, a language I do not speak at all. I tried conversing with them in Hindi, which is the national language but not the first language of either the NIOT workers or myself. Imagine me explaining what a χpod is in Hindi! I was waving my hands around as if I was acting out "ocean mixing" in a game of charades. Suffice to say, my descriptions of a wooden box and a χpod were met with confused stares.

"I quickly realized, however, that these were the very people who packed the container in the first place. So I pulled out my laptop from my bag, and showed them the Ocean Mixing Group sticker that I had serendipitously stuck to the cover, and told them 'Box pey yeh Sticker!' ('Sticker on the box' in Hindi/English).

"As soon as they saw the Ocean Mixing Group logo with its bold colors showing turbulence under a ship, they knew exactly which instruments I was talking about. They went in the container and immediately pulled out the two χpod boxes.

"Job done!"
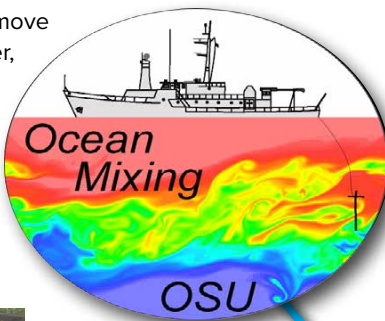
magnitude have been observed with other cyclones in the BoB (McPhaden et al., 2009a). TS Hudhud did not pass directly over the mooring and had yet to reach cyclone strength when it passed nearby; the observed temperature drop of 1.4°C suggests that vertical mixing and latent surface cooling elsewhere in the BoB was greater than measured at 12°N, 90°E.

The influence of TS Hudhud at the mooring extends over a 60-hour period from the time at which the wind stress began to increase, precipitation began to fall, and the sea surface began to cool on October 8, 2014, at midnight UTC (06:00 local time) until the wind stress died down and precipitation ended at noon UTC (18:00 local time) (Figure 7). During this period, the wind stress reached hourly averages of 0.8 N m^{-2} between 00:00 UTC and 04:00 UTC on October 9 (Figure 7a). Heavy precipitation occurred in the 24 hours preceding the maximum winds and in the last 12 hours of elevated wind stress. Summed over this 60-hour period, 95 mm of rain fell locally at 12°N, 90°E (Figure 7b).

Elevated winds and precipitation were accompanied by strong upward atmospheric heat flux (Figure 7c). Throughout October 8–10, J_q^0 was almost entirely negative, reaching rates as large as –340 W m^{-2}, 2.3 times larger than typical nighttime atmospheric cooling rates, but not as large as the latent heat flux observed during Cyclone Nargis, which reached a magnitude of –500 W m^{-2} (McPhaden et al., 2009a). Over this 60-hour period, J_q^0 averaged –193 W m^{-2} out of the ocean—enough to account for –0.68°C cooling of the mixed layer, assuming a 15 m deep mixed layer. (Note that no shortwave or longwave radiation data are available from the RAMA mooring at 12°N, 90°E during the passage of TS Hudhud; therefore, radiative fluxes from the mooring at 15°N, 90°E are used in combination with latent and sensible heat fluxes from 12°N. Hourly values from the 15°N mooring allow better visualization than daily averaged TropFlux fluxes in Figure 7.)

Determining the depth of cooling induced by TS Hudhud is accomplished by looking at temperature records from the RAMA mooring. The temperatures at 1 m and 10 m depth matched very closely throughout the passage of TS Hudhud (Figure 7d). Prior to the start of elevated winds on October 8, the temperature
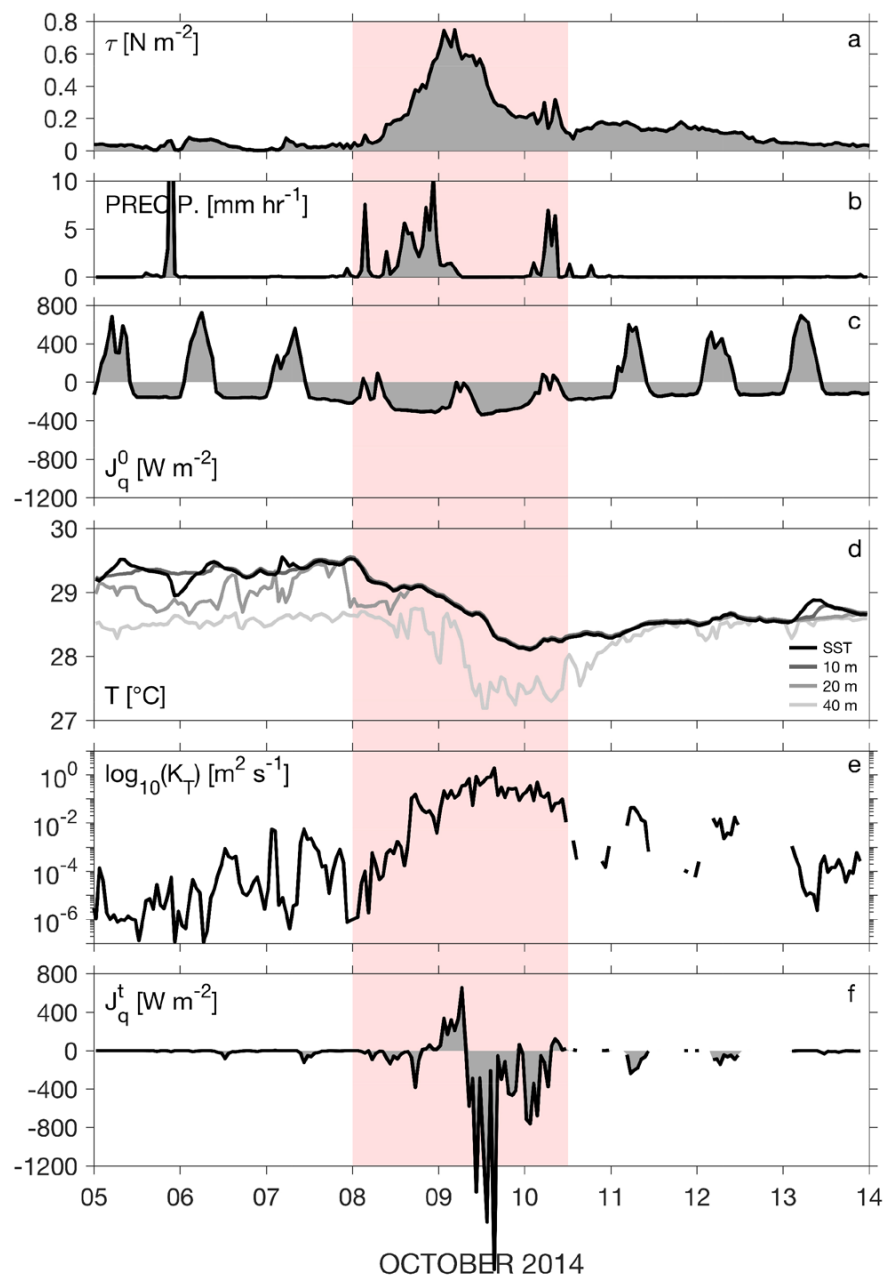

FIGURE 7. (a) Hourly averaged surface wind stress from the RAMA mooring at 12°N, 90°E from October 5–14, 2014. (b) Precipitation rate. (c) Atmospheric heat flux (J_q^0). Daily sensible and latent heat fluxes from the RAMA mooring at 12°N, 90°E are combined with hourly shortwave and longwave radiation from the RAMA mooring at 15°N, 90°E. Negative (positive) values indicate heat flux out of (into) the ocean. (d) Sea surface temperature (black) and subsurface temperatures at 10 m, 20 m, and 40 m depth (progressively lighter grays). (e) Turbulence diffusivity (K_T) as measured by a χpod at 15 m. (f) Turbulent heat flux (J_q^t) at 15 m. Positive (negative) values indicate upward (downward) heat flux that warms (cools) the surface waters. Gaps in K_T and J_q^0 following TS Hudhud occur when T_z decreases below 10^{-3} °C m^{-1}, at which point they are flagged due to lack of sufficient temperature stratification for χpod analysis. Background shading indicates passage of TS Hudhud based on wind stress magnitude and precipitation. Salinity is not plotted because it is only known at daily resolution.

at these depths was 29.5°C. A uniform drop in temperature of 1.4°C to 28.1°C occurred over October 8 and 9. In the days following the storm, the temperature between 1–10 m depth remained nearly a degree colder than it had been prior to the passage of TS Hudhud. Deeper temperatures did not follow the same pattern. It was not until nearly 17:00 UTC on October 8 that the 20 m temperature matched that of the shallower depths, indicating the time at which the mixed layer deepened to 20 m. From that point onward, 20 m temperatures fluctuated in concert with temperatures at shallower depths until restratification occurred on October 13. The temperature at 40 m depth decreased by 2°C from 28.8°C to 26.8°C between 02:00 UTC and 14:00 UTC on October 9, but remained colder than temperatures at shallower depths. This means that while TS Hudhud affected water at 40 m, the mixed layer did not extend to that depth. Furthermore, the temperature at 40 m depth returned nearly to its pre-storm level by October 11.

Turbulence diffusivities at 15 m depth increased by three orders of magnitude with the passage of TS Hudhud, reaching peak values at approximately the same time as maximum wind stresses, and remaining elevated until after the winds had died down (Figures 5 and 7e). The observed damping over the course of a few inertial periods after the passage of the storm is similar to observations elsewhere (Sanford et al., 2007).

Averaged over the 60-hour passage of TS Hudhud, J_q^0 contributed –193 W m^{-2} and J_q^t contributed –190 W m^{-2} of net cooling (Figure 7c,f), which combined to account for an equivalent SST change of –1.3°C over a 15 m layer. Over the first 30 hours, the majority of the average cooling was from the atmosphere: J_q^0 = –209 W m^{-2} of cooling versus J_q^t = +13 W m^{-2} of warming. This warming comes from the fact that the pre-storm temperature structure was negatively stratified, supported by stable salinity stratification. This is not uncommon; subsurface mixing during post-SW monsoon cyclones in the northern BoB have been observed to contribute to SST warming due to the presence of a barrier layer (Sengupta et al., 2008; Neetu et al., 2012). Once mixing eroded through the subsurface warm layer, cooling by turbulent mixing dominated atmospheric cooling during the subsequent 30 hours: J_q^t = –390 W m^{-2} compared to J_q^0 = –176 W m^{-2}. J_q^t accounted for 70% of the cooling during the latter half of TS Hudhud's passage. Initial surface warming followed by surface cooling as the barrier layer eroded was also observed during Cyclone Nargis in the BoB in 2008 (McPhaden et al., 2009a).

Large diffusivities and vertical heat fluxes indicate the important role vertical mixing plays in isolated events such as tropical cyclones. Furthermore, depending on the sign of the temperature stratification, subsurface mixing can alternately intensify or weaken a storm. Initially, release of heat trapped in subsurface warm layers may intensify storm development (Sengupta et al., 2008); however, in the absence of such heat reservoirs, sea surface cooling by subsurface mixing works to dampen the strength of storms. As subsurface ocean temperatures—in addition to SST—rise with climate change, the potential for this negative feedback mechanism is reduced (Emanuel, 2005).

SUMMARY

A year-long record of subsurface mixing at 12°N, 90°E in the BoB highlights processes that heat and cool sea surface temperatures during the NE and SW monsoons and during the passage of a tropical storm. During the NE monsoon, both atmospheric heat fluxes and subsurface turbulent heat fluxes worked to cool the sea surface, each contributing approximately –7 W m^{-2}. During the SW monsoon, daily averaged J_q^0 was characterized by both large negative and large positive values through active and break cycles, respectively, but had a net positive seasonal average of +30 W m^{-2}. The observed subsurface turbulent heat flux, which was nearly always negative during the SW monsoon, contributed a seasonal average of roughly –22 W m^{-2} of cooling. Averaged over the SW monsoon, the sea surface cools but J_q^0 contributes net warming, therefore subsurface turbulence must be an important mechanism working to decrease SST. During the low-wind, zero-precipitation transition between the NE and SW monsoons, turbulence levels were three orders of magnitude smaller than during the monsoons, and large atmospheric heating led to an SST increase of 4°C over two months. Throughout the year, occasional presence of barrier layers resulted in subsurface warming—rather than cooling—of the sea surface by J_q^t. With the passage of Tropical Storm Hudhud, the sea surface temperature decreased by 1.4°C over 60 hours. During the storm, the turbulent heat flux was roughly two orders of magnitude larger than at other times, and subsurface mixing and atmospheric heat fluxes contributed equally to the sea surface temperature decrease. 🔗

REFERENCES

Agarwal, N., R. Sharma, A. Parekh, S. Basu, A. Sarkar, and V.K. Agarwal. 2012. Argo observations of barrier layer in the tropical Indian Ocean. *Advances in Space Research* 50(5):642–654, http://dx.doi.org/10.1016/j.asr.2012.05.021.

Bhat, G.S., S. Gadgil, P.V. Hareesh Kumar, S.R. Kalsi, P. Madhusoodanan, V.S.N. Murty, C.V.K. Prasada Rao, V. Ramesh Babu, L.V.G. Rao, R.R. Rao, and others. 2001. BOBMEX: The Bay of Bengal Monsoon experiment. *Bulletin of the American Meteorological Society* 82(10):2,217–2,243, http://dx.doi.org/10.1175/1520-0477(2001)082<2217:BTBOBM>2.3.CO;2.

D'Asaro, E.A., T.B. Sanford, P.P. Niiler, and E. Terrill. 2007. Cold wake of Hurricane Frances. *Geophysical Research Letters* 34, L15609, http://dx.doi.org/10.1029/2007GL030160.

de Boyer Montégut, C., J. Vialard, S.S.C. Shenoi, D. Shankar, F. Durand, C. Ethé, and G. Madec. 2007. Simulated seasonal and interannual variability of the mixed layer heat budget in the northern Indian Ocean. *Journal of Climate* 20:3,249–3,268, http://dx.doi.org/10.1175/JCLI4148.1.

Emanuel, K. 2003. Tropical cyclones. *Annual Review of Earth and Planetary Sciences* 31(1):75–104, http://dx.doi.org/10.1146/annurev.earth.31.100901.141259.

Emanuel, K. 2005. Increasing destructiveness of tropical cyclones over the past 30 years. *Nature* 436:686–688, http://dx.doi.org/10.1038/nature03906.

Fritz, A. 2014. Deadly Tropical Cyclone Hudhud lashes India with winds over 100 mph. *Washington Post*, October 12, 2014, http://www.washingtonpost.com/news/capital-weather-gang/wp/2014/10/13/deadly-tropical-cyclone-hudhud-lashes-india-with-winds-over-100-mph.

Gadgil, S. 2003. The Indian monsoon and its variability. *Annual Review of Earth and Planetary Sciences* 31(1):429–467, http://dx.doi.org/10.1146/annurev.earth.31.100901.141251.

Gaulter, S. 2014. The powerful Cyclone Hudhud. *Gulf Times*, Doha, Qatar, October 19, 2014, http://www.gulf-times.com/story/412801/The-powerful-Cyclone-Hudhud.

Girishkumar, M.S., M. Ravichandran, and M.J. McPhaden. 2013. Temperature inversions and their influence on the mixed layer heat budget during the winters of 2006–2007 and 2007–2008 in the Bay of Bengal. *Journal of Geophysical Research* 118(5):2,426–2,437, http://dx.doi.org/10.1002/jgrc.20192.

Girishkumar, M.S., M. Ravichandran, M.J. McPhaden, and R.R. Rao. 2011. Intraseasonal variability in barrier layer thickness in the south central Bay of Bengal. *Journal of Geophysical Research* 116, C03009, http://dx.doi.org/10.1029/2010JC006657.

Goswami, B.N. 2011. South Asian monsoon. Pp. 21–72 in *Intraseasonal Variability in the Atmosphere-Ocean Climate System*. W.K.-M. Lau and D.E. Waliser, eds, Springer Science & Business Media.

Goswami, B.N., S.A. Rao, D. Sengupta, and S. Chakravorty. 2016. Monsoons to mixing in the Bay of Bengal: Multiscale air-sea interactions and monsoon predictability. *Oceanography* 29(2):18–27, http://dx.doi.org/10.5670/oceanog.2016.35.

Kalnay, E., M. Kanamitsu, R. Kistler, W. Collins, D. Deaven, L. Gandin, M. Iredell, S. Saha, G. White, J. Woollen, and others. 1996. The NCEP/NCAR 40-year reanalysis project. *Bulletin of the American Meteorological Society,* http://dx.doi.org/10.1175/1520-0477(1996)077<0437:TNYRP>2.0.CO;2.

Loschnigg, J., and P.J. Webster. 2000. A coupled ocean-atmosphere system of SST modulation for the Indian Ocean. *Journal of Climate* 13(19):3,342–3,360, http://dx.doi.org/10.1175/1520-0442(2000)013<3342:ACOASO>2.0.CO;2.

McPhaden, M.J., G.R. Foltz, T. Lee, V.S.N. Murty, M. Ravichandran, G.A. Vecchi, J. Vialard, J.D. Wiggert, and L. Yu. 2009a. Ocean-atmosphere interactions during Cyclone Nargis. *Eos, Transactions American Geophysical Union* 90(7):53–54, http://dx.doi.org/10.1029/2009EO070001.

McPhaden, M.J., G. Meyers, K. Ando, Y. Masumoto, V.S.N. Murty, M. Ravichandran, F. Syamsudin, J. Vialard, L. Yu, and W. Yu. 2009b. RAMA: The research moored array for African-Asian-Australian monsoon analysis and prediction. *Bulletin of the American Meteorological Society* 90(4):459–480, http://dx.doi.org/10.1175/2008BAMS2608.1.

Moum, J.N., and J.D. Nash. 2009. Mixing measurements on an equatorial ocean mooring. *Journal of Atmospheric and Oceanic Technology* 26(2):317–336, http://dx.doi.org/10.1175/2008JTECHO617.1.

Moum, J.N., A. Perlin, J.D. Nash, and M.J. McPhaden. 2013. Seasonal sea surface cooling in the equatorial Pacific cold tongue controlled by ocean mixing. *Nature* 500:64–67, http://dx.doi.org/10.1038/nature12363.

Neetu, S., M. Lengaigne, E.M. Vincent, J. Vialard, G. Madec, G. Samson, M.R. Ramesh Kumar, and F. Durand. 2012. Influence of upper-ocean stratification on tropical cyclone-induced surface cooling in the Bay of Bengal. *Journal of Geophysical Research* 117, C12020, http://dx.doi.org/10.1029/2012JC008433.

Perlin, A., and J.N. Moum. 2012. Comparison of thermal variance dissipation rates from moored and profiling instruments at the equator. *Journal of Atmospheric and Oceanic Technology* 29(9):1,347–1,362, http://dx.doi.org/10.1175/JTECH-D-12-00019.1.

Praveen Kumar, B., J. Vialard, M. Lengaigne, V.S.N. Murty, and M.J. McPhaden. 2012. TropFlux: Air-sea fluxes for the global tropical oceans: Description and evaluation. *Climate Dynamics* 38:1,521–1,543, http://dx.doi.org/10.1007/s00382-011-1115-0.

Reynolds, R.W., T.M. Smith, C. Liu, D.B. Chelton, K.S. Casey, and M.G. Schlax. 2007. Daily high-resolution-blended analyses for sea surface temperature. *Journal of Climate* 20(22):5,473–5,496, http://dx.doi.org/10.1175/2007JCLI1824.1.

Sanford, T.B., J.F. Price, J.B. Girton, and D.C. Webb. 2007. Highly resolved observations and simulations of the ocean response to a hurricane. *Geophysical Research Letters* 34, L13604, http://dx.doi.org/10.1029/2007GL029679.

Schott, F.A., and J.P. McCreary. 2001. The monsoon circulation of the Indian Ocean. *Progress in Oceanography* 51(1):1–123, http://dx.doi.org/10.1016/S0079-6611(01)00083-0.

Schott, F.A., S.-P. Xie, and J.P. McCreary Jr. 2009. Indian Ocean circulation and climate variability. *Reviews of Geophysics* 47:1–46, http://dx.doi.org/10.1029/2007RG000245.

Sengupta, D., B.R. Goddalehundi, and D.S. Anitha. 2008. Cyclone-induced mixing does not cool SST in the post-monsoon north Bay of Bengal. *Atmospheric Science Letters* 9(1):1–6, http://dx.doi.org/10.1002/asl.162.

Sengupta, D., B.N. Goswami, and R. Senan. 2001. Coherent intraseasonal oscillations of ocean and atmosphere during the Asian summer monsoon. *Geophysical Research Letters* 28(21):4,127–4,130, http://dx.doi.org/10.1029/2001GL013587.

Sengupta, D., and M. Ravichandran. 2001. Oscillations of Bay of Bengal sea surface temperature during the 1998 summer monsoon. *Geophysical Research Letters* 28(10):2,033–2,036, http://dx.doi.org/10.1029/2000GL012548.

Sengupta, D., P.K. Ray, and G.S. Bhat. 2002. Spring warming of the eastern Arabian Sea and Bay of Bengal from buoy data. *Geophysical Research Letters* 29(15), http://dx.doi.org/10.1029/2002GL015340.

Shenoi, S.S.C., D. Shankar, and S.R. Shetye. 2002. Differences in heat budgets of the near-surface Arabian Sea and Bay of Bengal: Implications for the summer monsoon. *Journal of Geophysical Research* 107(C6), http://dx.doi.org/10.1029/2000JC000679.

Syed, F.S., W. Iqbal, A.A.B. Syed, and G. Rasul. 2014. Uncertainties in the regional climate models simulations of South-Asian summer monsoon and climate change. *Climate Dynamics* 42:2,079–2,097, http://dx.doi.org/10.1007/s00382-013-1963-x.

Thadathil, P., V. Gopalakrishna, P. Muraleedharan, G. Reddy, N. Araligidad, and S. Shenoy. 2002. Surface layer temperature inversion in the Bay of Bengal. *Deep Sea Research Part I* 49(10):1,801–1,818, http://dx.doi.org/10.1016/S0967-0637(02)00044-4.

Thadathil, P., P.M. Muraleedharan, R.R. Rao, Y.K. Somayajulu, G.V. Reddy, and C. Revichandran. 2007. Observed seasonal variability of barrier layer in the Bay of Bengal. *Journal of Geophysical Research* 112, C02009, http://dx.doi.org/10.1029/2006JC003651.

Thangaprakash, V.P., M.S. Girishkumar, K. Suprit, N. Suresh Kumar, D. Chaudhuri, K. Dinesh, A. Kumar, S. Shivaprasad, M. Ravichandran, J.T. Farrar, and others. 2016. What controls seasonal evolution of sea surface temperature in the Bay of Bengal? Mixed layer heat budget analysis using moored buoy observations along 90°E. *Oceanography* 29(2):202–213, http://dx.doi.org/10.5670/oceanog.2016.52.

The Economic Times. 2015. Cyclone Hudhud causes $11 billion worth of losses: UN. February 26, 2015, http://articles.economictimes.indiatimes.com/2015-02-26/news/59541541_1_natural-disasters-asia-pacific-region-cyclone-hudhud.

The Times of India. 2014. Hudhud killed 46 in Andhra Pradesh, 21 lakh families hit. October 25, 2014, http://timesofindia.indiatimes.com/india/Hudhud-killed-46-in-Andhra-Pradesh-21-lakh-families-hit/articleshow/44932425.cms.

Toole, J.M., K.L. Polzin, and R.W. Schmitt. 1994. Estimates of diapycnal mixing in the abyssal ocean. *Science* 264:1,120–1,123, http://dx.doi.org/10.1126/science.264.5162.1120.

Wang, S.-Y., R.R. Gillies, B. Fosu, and P.M. Singh. 2015. The deadly Himalayan snowstorm of October 2014: Synoptic conditions and associated trends [in "Explaining Extreme Events of 2014 from a Climate Perspective"]. *Bulletin of the American Meteorological Society* 96(12):89–94, http://dx.doi.org/10.1175/BAMS-D-15-00113.1.

Weller, R.A., J.T. Farrar, J. Buckley, S. Mathew, R. Venkatesan, J. Sree Lekha, D. Chaudhuri, N. Suresh Kumar, and B. Praveen Kumar. 2016. Air-sea interaction in the Bay of Bengal. *Oceanography* 29(2):28–37, http://dx.doi.org/10.5670/oceanog.2016.36.

Yu, L., X. Jin, and R.A. Weller. 2007. Annual, seasonal, and interannual variability of air–sea heat fluxes in the Indian Ocean. *Journal of Climate* 20(13):3,190–3,209, http://dx.doi.org/10.1175/JCLI4163.1.

Yu, L., and M.J. McPhaden. 2011. Ocean preconditioning of Cyclone Nargis in the Bay of Bengal: Interaction between Rossby waves, surface fresh waters, and sea surface temperatures. *Journal of Physical Oceanography* 41(9):1,741–1,755, http://dx.doi.org/10.1175/2011JPO4437.1.

Yu, L., and R.A. Weller. 2007. Objectively analyzed air-sea heat fluxes for the global ice-free oceans (1981–2005). *Bulletin of the American Meteorological Society* 88(4):527–539, http://dx.doi.org/10.1175/BAMS-88-4-527.

AUTHORS

Sally J. Warner (swarner@coas.oregonstate.edu) is Research Associate, **Johannes Becherer** is Research Associate, **Kandaga Pujiana** is Research Associate, and **Emily L. Shroyer** is Assistant Professor, all in the College of Earth, Ocean, and Atmospheric Sciences, Oregon State University, Corvallis, OR, USA. **M. Ravichandran** is Head, Observations and Modeling, and **V.P. Thangaprakash** is Scientist, both at the Indian National Center for Ocean Information Services, Hyderabad, India. **James N. Moum** is Professor, College of Earth, Ocean, and Atmospheric Sciences, Oregon State University, Corvallis, OR, USA.